INTERFACE

rsif.royalsocietypublishing.org

Research

Cite this article: Quandt BM *et al*. 2017 Body-monitoring with photonic textiles: a reflective heartbeat sensor based on polymer optical fibres. *J. R. Soc. Interface* **14**: 20170060. http://dx.doi.org/10.1098/rsif.2017.0060

Received: 26 January 2017
Accepted: 10 February 2017

Subject Category:
Life Sciences–Engineering interface

Subject Areas:
medical physics, biomedical engineering

Keywords:
long-term monitoring, polymer optical fibres, photoplethysmography, melt-spinning, biomedical optics

Author for correspondence:
Luciano F. Boesel
e-mail: luciano.boesel@empa.ch

Electronic supplementary material is available online at https://dx.doi.org/10.6084/m9.figshare.c.3710527.

THE ROYAL SOCIETY PUBLISHING

Body-monitoring with photonic textiles: a reflective heartbeat sensor based on polymer optical fibres

Brit M. Quandt[1,2], Fabian Braun[3], Damien Ferrario[3], René M. Rossi[1], Anke Scheel-Sailer[4], Martin Wolf[5], Gian-Luca Bona[1,2], Rudolf Hufenus[1], Lukas J. Scherer[1] and Luciano F. Boesel[1]

[1]Empa, Swiss Federal Laboratories for Materials Science and Technology, Lerchenfeldstrasse 5, 9014 St Gallen, Switzerland
[2]Department of Information Technology and Electrical Engineering, ETH Zurich, Swiss Federal Institute of Technology, Gloriastrasse 35, 8092 Zurich, Switzerland
[3]CSEM, Swiss Center for Electronics and Microtechnology, Rue Jaquet-Droz 1, 2002 Neuchâtel, Switzerland
[4]Swiss Paraplegic Center, Guido A. Zäch Strasse 1, 6207 Nottwil, Switzerland
[5]Biomedical Optics Research Laboratory, Department of Neonatology, University Hospital Zurich, Frauenklinikstrasse 10, 8091 Zurich, Switzerland

BMQ, 0000-0002-1553-6655; LFB, 0000-0003-4481-9651

Knowledge of an individual's skin condition is important for pressure ulcer prevention. Detecting early changes in skin through perfusion, oxygen saturation values, and pressure on tissue and subsequent therapeutic intervention could increase patients' quality of life drastically. However, most existing sensing options create additional risk of ulcer development due to further pressure on and chafing of the skin. Here, as a first component, we present a flexible, photonic textile-based sensor for the continuous monitoring of the heartbeat and blood flow. Polymer optical fibres (POFs) are melt-spun continuously and characterized optically and mechanically before being embroidered. The resulting sensor shows flexibility when embroidered into a moisture-wicking fabric, and withstands disinfection with hospital-type laundry cycles. Additionally, the new sensor textile shows a lower static coefficient of friction (COF) than conventionally used bedsheets in both dry and sweaty conditions versus a skin model. Finally, we demonstrate the functionality of our sensor by measuring the heartbeat at the forehead in reflection mode and comparing it with commercial finger photoplethysmography for several subjects. Our results will allow the development of flexible, individualized, and fully textile-integrated wearable sensors for sensitive skin conditions and general long-term monitoring of patients with risk for pressure ulcer.

1. Introduction

Many complex health conditions, e.g. pressure ulcer prevention, require unobtrusive long-term monitoring to register developing wounds early. The changes in skin and underlying tissue vary strongly between individuals and not much data are available so far. People prone to development would benefit from individual feedback and personalized therapeutic intervention. Information on the perfusion of the skin, the oxygen saturation and pressure levels on the tissue could allow for understanding on tissue changes over time. With long-term data on all three of those parameters, the intervention protocol could then be adjusted to the individual's pressure tolerance curve (depending e.g. on the breakdown of microvasculature) [1].

While these diseases need supervision, hospitals often do not have the capacity to monitor these patients at all times [2]. Additionally, the available flexible options (e.g. incorporated printed circuit boards) are often still bulky and cannot be used as they create additional pressure spots and skin chafing

[1,3,4]. These pressure spots then increase the risk of injury. Additional threats to skin health, including irritation, injury and inflammation have to be avoided. With these prerequisites, the development of textile sensors for long-term measurements becomes essential.

Therefore, we present one component of such a flexible monitoring tool: a photonic textile sensor logging the heartbeat via a photoplethysmography (PPG) signal. This sensor is specifically designed for sensitive skin to prevent (further) injury by only incorporating soft polymer optical fibres (POFs). Recently, development regarding polymer optical fibres for healthcare monitoring has increased greatly [5]. The decreased attenuation adds to the advantage of often higher flexibility compared with glass fibres [6,7]. As POF can possess yarn-like flexibility, much more flexible and drapeable sensors can be produced and incorporated into textiles [8,9]. Development of another sensor important to this application—a flexible, pressure-sensitive polymer optical fibre—has recently been published elsewhere [9].

This textile production requires not only high flexibility of the fibres but also toughness to continue guiding light after production of the textile. Therefore, we present the development and optimization of bi-component polymer optical fibres by continuous melt-spinning, a fast process rendering continuous fibres. The co-extruded sheath serves here as the optical cladding to a step-index profile POF. Therefore, when discussing the application, the traditional term for POF, cladding, is used.

The heartbeat sensors were produced by embroidery which ensures small bending radii and strong bend light out-coupling from the POFs [5,8]. The increased light intensity allows for a stronger PPG signal through the tissue. Owing to the improved optical properties of these POFs, we were able to verify that the previously used laser light sources were omitted for commercial LEDs, eliminating laser safety restrictions [8].

Besides light in- and out-coupling, comfort is another important property for textile sensors. Earlier work demonstrated a good correlation between the friction coefficient and the tactile impression [10,11]. Additionally, it has to be kept in mind that an entirely textile structure will produce a different skin climate than a non-breathable rigid sensor. The wearing comfort, including the transport of sweat away from the skin, can be expected to differ. The removal of fluids from the skin is beneficial for ulcer prevention, especially with the development of the coefficient of friction (COF) from the dry to the wet state in mind [12].

Finally, reusability is another important factor in sensor development. The possibility of reusing a sensor makes it economically and ecologically more favourable by decreasing the per-patient cost drastically. Hence, a reusable, washable sensor decreases health cost such as targeting a current issue in household spendings [13]. In the medical sector, safe hygienic conditions have to be ensured, which then limits development to washable sensors [14].

The newly developed fabrics are evaluated in friction and hence dermatologic tolerance. This is performed in comparison with its substrate and other reference textiles against a commercially available skin model. The sensor is designed to work in reflection mode. This set-up does not require light transmission and can hence be used on any body part. In the last few years, we have presented a range of photonic textile sensors for the long-term monitoring of pressure, breathing rate and heart rate [8,15,16]. The last two have successfully been validated against commercial devices, with a good correlation in acquired data. The heart beat sensor, however, still presents some drawbacks limiting its effective use in clinics: the in-coupling of light into the tissue is done by using a conventional PMMA optical fibre, which is stiff and cumbersome when integrated into the textile [8]. It may therefore lead to low comfort due to high friction and/or skin chafing. Therefore, only the flexible-specialty POFs are used for the new design. The functionality of the sensor is additionally tested after hospital-type washing cycles to guarantee its reusability. For existing wounds, the sensor can be used to determine skin perfusion, which gives information on wound healing.

2. Experimental section

This paper comprises the development of a textile heartbeat sensor from the production of the sensing component, the POFs, to the subject testing of the sensor. This comprises melt-spinning of a bi-component fibre, evaluation of these in homogeneity, as well as optical and mechanical properties, textile integration, comfort evaluation and testing. 'Comfort' is, in this case, defined by the static COF because the targeted patient group typically adheres to strict safety standards to prevent skin chafing.

2.1. Melt-spinning of optical fibres

For the production of the bi-component polymer optical fibres, a continuous fibre spinning process was used [17,18]. The core-cladding-structure was produced by simultaneously spinning two polymers with a melt-spinning plant by Fourné Polymertechnik (Alfter-Impekoven, Germany) [17]. Two single screw extruders (18×25 D for the core and 13×25 D for the sheath) were used to process and force the two polymers through a bi-component die with inner diameter 1.2 mm, containing a capillary with 0.7 mm outer and 0.4 mm inner diameter. The fibre was cooled in a quenching chamber and three godets were used for drawing. Fibre collection was carried out with a winder as described in a previous publication [19]. The draw ratio, namely the ratio between the winder speed and that of the take-up godet, was varied between 1 and 2.

The core polymer Zeonor 1020R (COP) was acquired from Zeon Chemicals (Louisville, KY, USA), while the sheath polymer THVP-2030G × (THV) is produced by Dyneon GmbH & Co. KG (Burgkirchen, Germany). Their densities are given as 1.01 g cm^{-3} and 1.98 g cm^{-3}, respectively. Before usage, the COP and THV were dried at 100°C and 90°C, respectively in a vacuum oven for at least 12 h. During production, their temperatures at the dye were both 250°C. Further specifications can be taken from table 1.

During the melt-spinning process, light attenuation was monitored for processing changes with a medical laser diode at 652 nm at an intensity of 100 mW (Applied Optronics, South Plainfield, NJ, USA) using the cutback method. The fibres were connected to a mode mixer via F-SMA connectors (Thorlabs, Newton, NJ, USA). The output was logged by using an integrating sphere UM-150 (Gigahertz-Optik GmbH, Türkenfeld, Germany) and a photomultiplier tube (PRC Krochmann, Berlin, Germany). Optimization of production parameters was performed iteratively to receive

Table 1. Production parameters of the bi-component polymer optical fibre ID-1143 and ID-1144.

fibre no.	polymer		c/s	core	godet 1		godet 2		godet 3		winder	
	core	sheath	vol. ratio	wt%	speed (m min^{-1})	temp. (°C)	speed (m min^{-1})	temp. (°C)	speed (m min^{-1})	temp. (°C)	speed (m min^{-1})	draw ratio
ID-1143	COP	THV	2	51	300	40	305	40	310	40	305	1
ID-1144	COP	THV	2	51	200	40	300	90	400	40	395	2

low-loss fibres and improve previously produced fibres regarding homogeneity and mechanical performance [8,17].

2.2. Homogeneity and mechanical characterization of the optical fibres

The fibres were evaluated in homogeneity by scanning electron microscopy (SEM) (Hitachi S-4800, Hitachi, Ltd., Tokyo, Japan) after being embedded in epoxy, polished perpendicularly, and afterwards coated with gold-palladium (10 nm) with a Leica EM ACE600 high-vacuum sputter coater (Leica Microsystems, Wetzlar, Germany). The SEM was operated at a voltage of 5 kV and 10 µA beam current. Additionally, cross-sections, prepared without the coating, were evaluated under a Keyence VHX-1000 Multiscan microscope (Osaka, Japan).

The tensile properties of the fibres were evaluated with the Statimat ME+ (textechno Herbert Stein GmbH & Co. KG, Mönchengladbach, Germany) with a 100 N load cell at 600 mm min^{-1} drawing speed. The measurements for each fibre type were repeated 20 times. Hence, the standard deviation of the nominal stress was calculated by error propagation taking the standard deviation of both the initial fibre radius and the variation along the fibre axis into account.

Two further experiments were performed in relation to the mechanical performance of the fibres: knot efficiency as well as bending resiliency. The knot efficiency was used to determine whether these fibres can be used for embroidery. For bending resiliency, however, the recovery was important for determining whether plastic deformation takes place during embroidery. Plastic deformation of the fibre increases light out-coupling at that location. The knot efficiency was also tested on the same machine with 20 repetitions. For knot efficiency, the ratio of the strength at break of a knotted fibre and the virgin fibre are compared. The knots were pre-tensioned by applying a 25 g weight which lies below the tensile modulus of both fibres. It was not necessary to differentiate between Z- and S-knots as the POF shows no yarn twist. To measure resiliency of the fibres under bending, a lever was lowered onto a horizontally placed fibre end. The end is gradually bent down by the lever at a bending radius of 3 mm and finally released. The fibre end then returned from a bent state towards its initial position. This movement was recorded by a high-speed camera and resiliency was calculated from angle differences between initial and current position at different time frames [20]. For these experiments, a Zwick Z100 with a 100 N load cell was used (Zwick Roell Group, Ulm, Germany).

2.3. Attenuation spectra of optical fibres

Optical fibre attenuation spectra were measured by the cut-back method using an Andor Shamrock spectrograph 303i-A (Andor Technology Ltd, Belfast, UK) equipped with a high-speed CCD camera (iDus DV 420A-OE, Andor). With a 20 µm slit setting and 750 nm centring, the measured range is 465.2–1034.1 nm. The lamp SLS201/M (Thorlabs Inc., Newton, NJ, USA) provides 300–2600 nm wavelengths with a stabilized tungsten-halogen light source. Additionally, an optical density filter of 2.0 and a 550 nm long-pass filter (ND20B and FGL550, both Thorlabs) were added at the source. The spectra were hence taken from 600 to 1000 nm,

Table 2. Diameter of core and cladding for virgin and washed optical fibres; for the washed fibres ID-1144, the detergent content varies, either 0 or 4 g l^{-1} were used to also investigate detergent effect. (i) Obtained by SEM images, (ii) obtained from optical microscope images. All data regarding fibre ID-1144 were obtained by the same spool of fibre. Statistical analysis: (i) fibres ID-1143 × ID-1144. *Value significantly different than that for fibre ID-1144 ($p < 0.05$). **Value significantly different than that for fibre ID-1144 ($p < 0.01$). (ii) Effect of washing: superscripts a and b identify samples (in the same line) which do not show significant differences for the corresponding property ($p < 0.01$).

	virgin fibre ID-1143[(i)]	virgin fibre ID-1144[(i)]	ID-1144 – 0 g 250 ml^{-1} [(ii)]	ID-1144 – 1 g/250 ml^{-1} [(ii)]
diameter cladding (μm)	179 ± 11**	161 ± 6[a]	157 ± 5[a,b]	156 ± 4[b]
diameter core (μm)	156 ± 9**	141 ± 6[a]	136 ± 4[b]	136 ± 3[b]
distance centres (μm)	4.2 ± 1.0*	3.7 ± 1.1[a]	2.1 ± 0.5[b]	2.0 ± 0.5[b]
flattening cladding (%)	4.0 ± 1.9	4.4 ± 1.9	—	—
flattening core (%)	4.5 ± 1.7*	3.7 ± 2.1	—	—

600 nm showing full transmittance through the long-pass filter [21]. Connection to the device under test (DUT) was ensured by two commercial optical fibres (type M14L02 (50 μm diameter) and type M25L02 (200 μm diameter), both Thorlabs). Both fibres were unjacketed, spliced and connected to the DUT with a droplet of index-matching liquid. The light intensity was maximized by aligning both *xyz*-stages in regard to the tested fibre. The schematic can be seen in electronic supplementary material, figure S1 (left). The determination of fibre axis for optimized fibre coupling takes the difference of fibre diameters into account (LabVIEW program (National Instruments Switzerland GmbH, Ennetbaden, Switzerland) written by Eugen Zgraggen) [22]. A schematic of coupled power at different scanning positions can be seen in electronic supplementary material, figure S1 (right).

Spectrometer data were then recorded at the highest possible integration time without saturation (less than or equal to 60 000 counts) for optimum signal-to-noise ratio.

2.4. Sensor embroidery

Embroidery was performed on a low-friction bedsheet (Schoeller Textil AG, Sevelen, Switzerland) as a substrate. This textile was designed for decubitus ulcer prevention and hence deemed a suitable substrate for this study [23]. A Saurer Era (SAURER Inc., Arbon, Switzerland), provided by Forster Rohner AG, textile innovations (St Gallen, Switzerland), was used. The textile was tensioned to 108.1% and 105.3% in the *x*- and the *y*-directions, respectively, with appropriate scaling to the correct pattern size after release. Additionally, yarn tension of both bobbin yarn (Pes 80/2 textured) and POF (monofilament ID-1144) was monitored.

2.5. Friction analysis of the sensor

The skin-fabric interface is simulated by the developed fabric with a mechanical skin model [24]. For the model, Lorica soft® (Lorica Sud, Milan, Italy) was applied as it corresponds well to the roughness and surface topography of human skin [25]. For each measurement, a new skin model was used. The samples were tested for 1000 cycles at a load of 8.5 N (=13.3 kPa) which lies within the range of typical interface pressures at the ischial tuberosities [1]. The mean static COF was calculated by averaging 50 cycles and four repetitions per condition. The stroke length was 20 mm with an oscillation frequency of 1.25 Hz.

For the friction measurements, three different designs were used. The embroidered structures covered 64.4%, 80.2% and 100% (6.4 cm^2) of the measurement patch. The additional measurements in wet conditions were performed by applying 64 μl of deionized water on the skin model to simulate extreme moisture (e.g. heavy sweating) [26]. All tests were performed in standard climate conditions (20 ± 1°C, 65 ± 2%RH).

2.6. Washing tests of the sensor

Evaluation of the sensor was done both through side light out-coupling intensity as well as monitoring the cross-sections of the fibres, the latter also being evaluated statistically in table 2.

Laundry tests were performed on a Roaches Washtec-P TPC 3002 (Birstall, UK) according to the protocol given by EN ISO 105-C06 : 1997 A1M at 40°C for 45 min, the effective temperature of the detergent. A hospital-grade industrial powder detergent was used containing oxygen bleach [27]. The sample was washed with 4 g of detergent per litre of deionized water within a plastic bottle. The sample holder was attached to a rotating shaft that immersed the sample into the heated water tank. After washing, the sample was removed from the solution, rinsed with deionized water and dried at air.

The normalized light out-coupling intensity from a red LED ($\lambda_{peak} = 660$ nm, E97, Industrial Fiber Optics, Tempe, AZ, USA) was evaluated along the embroidered lines with an optometer (P9710, Gigahertz-Optik GmbH, Türkenfeld, Germany) as seen in figure 3*a*. The measurements were repeated five times to take connector variability into account. Propagation of error was considered for the standard deviations in determining the light emission over the entire textile. The used detector covers from 400 to 1000 nm (RW-3705-2, SN21103).

2.7. Heartbeat sensor testing

The produced sensor (figure 5) was tested with dedicated electronics based on the PPG acquisition chain. PPG detects blood volume changes by utilizing the absorption of light by haemoglobin. At larger blood volumes (e.g. with each heart beat), a signal reaching the detector is decreased. The waveform shows the pulsatile component of the heart beat while being superimposed on a baseline. The former is caused by the changes with each heart beat while the latter

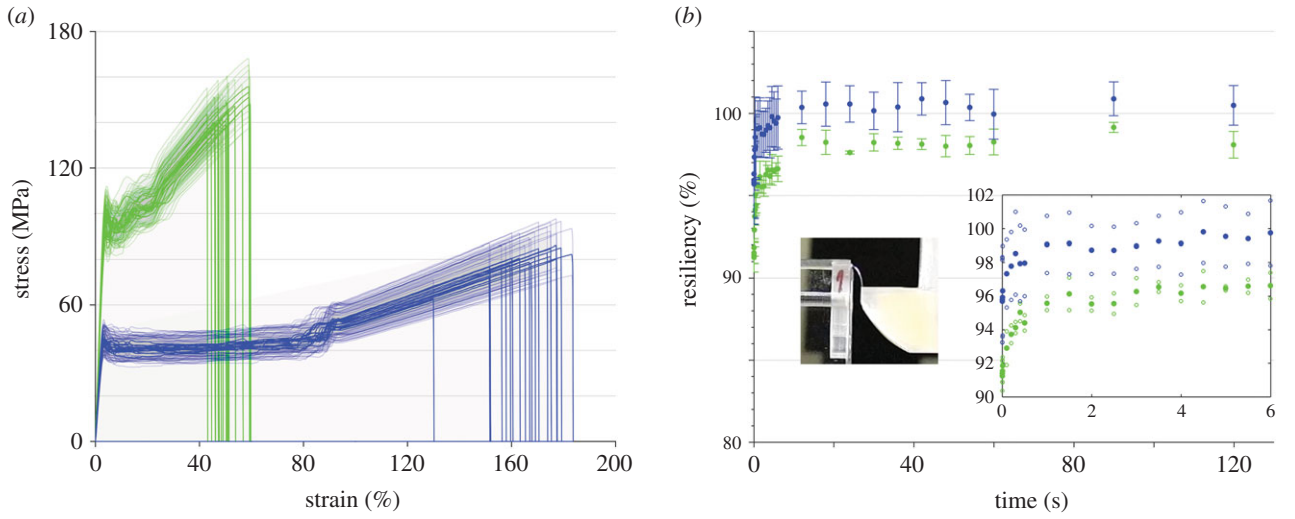

Figure 1. (*a*) Mechanical testing of the polymer optical fibres ID-1143 (blue) and ID-1144 (green), the plotted standard deviation arises from the error in (initial) radii of the fibres when converting to stress; (*b*) resiliency of the optical fibres to bending at a bending radius of 3 mm. Fibre ID-1143 is plotted in blue while fibre ID-1144 is plotted in green. The inset shows the set-up at the point just before release of the fibre as well as a plot of the first 6 s of recovery (solid dots), with the lower and upper standard deviation given also for each point (vacant dots).

is caused by lower-frequency components [28,29]. The connection between the electronic and the optical fibre was obtained using a commercial infrared LED ($\lambda = 870$) and a phototransistor (gain of 100 A/W) from Industrial Fiber Optics (Tempe, AZ, USA), part IF-E91D and IF-D92, respectively. The heartbeat was recorded from the forehead in reflection mode. The sensor was fixed to the head with a headband. The measurement protocol for comparison of the sensors included recording of a baseline (1 min), two isometric handgrip exercises at approximately 40% maximum voluntary contraction over 1 and 1.5 min as well as 1.5 min of deep breathing, both leading to modulation of heart rate. The subject was sitting on a chair and reference heart beat was synchronously measured with a fingertip PPG sensor connected to the BIOPAC MP150 (Biopac Systems Inc., USA). The verification was repeated for five subjects.

2.8. Statistical data analysis

Statistical data analysis was performed on acquired data with the 'R' program and the 'R-commander' package [30,31]. Shapiro–Wilk tests were used to test for the normality of the samples; afterwards differences in the central values of two samples were tested by using the Student *t*-test (for samples following the normal distribution) or the Mann–Whitney *U*-test (otherwise). One-way analysis of variance (ANOVA) was used to test for differences in means of groups of samples following the normal distribution, with Tukey contrasts being subsequently used for the multiple comparisons of means. In case of non-normal samples, we applied the Kruskal–Wallis rank sum tests and pairwise Wilcoxon rank sum tests, respectively. The analysis results are noted at the respective images or tables.

3. Results and discussion

3.1. Homogeneity and mechanical characterization of the optical fibres

We produce two POFs, named ID-1143 and ID-1144, via melt-spinning. While the draw ratio of ID-1143 is 1, ID-1144 is drawn to a ratio of 2. Both fibres show good roundness with a flattening of maximum 4.5% of both core or optical cladding. However, with the flattening of the core significantly lower for fibre ID-1144 ($p < 0.05$), the interface of core and optical cladding is more homogeneous along the fibre axis. Additionally to the roundness, the core is off-centred within the sheath by only 4.2 µm (ID-1143) and 3.7 µm (ID-1144) (table 2). Deviations in the core weight percentage between produced fibres and the extrusion settings occurred due to gear pump throughput. The throughput is dependent among others on the polymer viscosity. Seeing that the fibres were produced at high temperature, densities of polymers can differ greatly from the data sheet value at room temperature [32,33]. Therefore, the calculated value from the extruder control deviates from the obtained fibres.

Fibre ID-1144 shows slightly lower standard deviations in both core and optical cladding possibly due to the hot drawing, evening the fibre. The influence of drawing a fibre also carries into the tensile properties. While the drawn fibre shows a much larger tensile modulus, the average elongation at break lies below one third of the undrawn fibre (figure 1*a*). Both fibres show small error within their tensile properties, underlining their good homogeneity. Fibre ID-1144 shows even lower standard deviation of the elongation at the break, possibly due to less spinning instabilities (table 3). These decrease with higher drawing ratio.

The stress–strain graphs (figure 1*a*) show the upper yield point as well as plastic deformation and subsequent strain hardening starting at approximately 90% for ID-1143. Fibre ID-1144 is drawn during production and hence already plastically deformed [34]. After the upper yield point, minor fluctuations between residual plastic deformation and strain hardening can be seen. Additional tests have been performed as can be seen in electronic supplementary material, figure S2 with pre-drawn fibres. With pre-drawn fibres to 26% strain, these fluctuations are eliminated. For these experiments, the initial radius was adjusted to an average 71.7 µm (because the fibres were elongated). This value was then used for stress calculations.

In the context of its later application area, the knot efficiency of the fibres has also been evaluated. Seeing that

Table 3. Tensile properties of both fibres ID-1143 and ID-1144 in their virgin state as well as when knotted with tensioning of 25 g. Statistical analysis. The following two-sample comparisons have been performed for the three investigated tensile properties: (i) fibres ID-1143 × ID-1144, all properties present significantly different values ($p < 0.01$); (ii) fibres ID-1143 knotted × ID-1144 knotted, all properties present significantly different values ($p < 0.01$); (iii) fibres ID-1143 × ID-1143 knotted, properties with significant differences are marked with superscript a; (iv) fibres ID-1144 × ID-1144 knotted, properties with significant differences are marked with superscript b.

	tensile modulus (MPa)	ultimate tensile strain (%)	ultimate tensile stress (MPa)	knot efficiency (%)
ID-1143	16.9 ± 0.7[a]	165.6 ± 12.4	79.2 ± 5.3	98.1 ± 0.3
ID-1143—knotted	12.7 ± 0.8	170.4 ± 14.8	77.7 ± 5.4	
ID-1144	30.1 ± 1.3[b]	51.1 ± 5.3	144.6 ± 5.0[b]	95.9 ± 1.4
ID-1144—knotted	22.7 ± 1.8	49.4 ± 6.9	138.6 ± 6.8	

both fibres show high knot efficiency (the strength at break of the knotted fibre) above 96% of the straight one, they were deemed resistant enough for embroidery (table 3). Fibre ID-1143 shows higher resiliency to bending, reaching 100% within 12 s (figure 1*b*). From this, we can conclude that fibre ID-1143 is not plastically deformed at a bending radius of 3 mm, comparing to sole COP fibres [20]. Even with an optical cladding, the good resiliency of the COP material is preserved. Fibre ID-1144 returns to its maximum value also within 12 s; however, it does not recover fully. This speaks for the onset of plastic deformation and hence some plastic deformation during embroidery. The lower resiliency compared with the undrawn fibre could be explained by its drawn state and hence higher stiffness as well as the lower diameter which influences bending stress.

3.2. Attenuation spectra of optical fibres

In order to verify usage of the flexible optical fibres in both visible and near-infrared wavelengths applications, the attenuation spectra were measured via the cutback method. The full spectrum can already give information for further applications using several wavelengths, e.g. oxygen saturation measurements. Figure 2 shows the attenuation loss for both fibres. The drawn fibre (ID-1144) shows overall lower attenuation but similar peak positions. Comparing with glass fibres for communication systems as well as PMMA fibres, the attenuation is higher in most regions; however, in such a short transmission range sensor, the flexibility could outweigh even higher attenuation. Still, for an appropriate signal-to-noise ratio, the attenuation should be minimized. The fibres were designed to be extremely flexible and resilient (as discussed in the previous section, figure 1). To this, cyclo-olefins as well as fluoropolymers add with their low moisture uptake [35]. The newly produced fibres also compare well with our previous study (measured at 652 nm) [17].

Generally, losses stem from either intrinsic or extrinsic absorption. Extrinsic losses increase due to e.g. bubble generation in the core during production, surface roughness, an inhomogeneous interface between core and optical cladding or impurities. Intrinsic absorption in the infrared regions is mainly caused by the characteristic vibration frequencies of atomic bonds. C–C stretching vibrations can be expected from 1000 nm, as can be noted at the upper end of the spectrum [36]. C–H stretching vibrations occur around 550, 630, 740 and 900 nm and can be expected to make an impact on

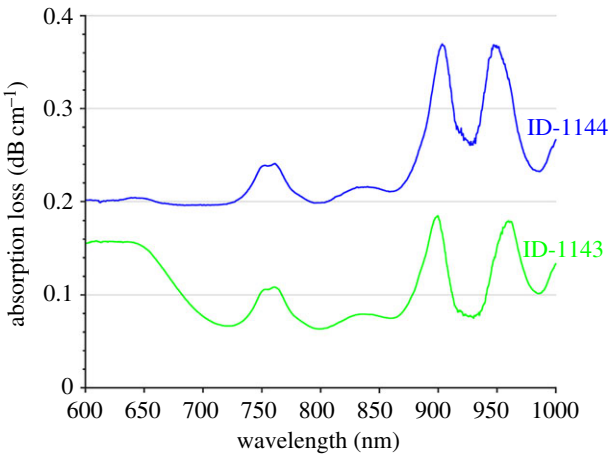

Figure 2. Attenuation spectrum from 600 to 1000 nm for the two polymer optical fibres, ID-1143 and ID-1144. (Online version in colour.)

the attenuation loss [36,37]. The differing behaviour of the two fibres around 600 nm could arise from C–F vibrations and hence an influence of the optical cladding on the absorption spectrum. [36] With the more pronounced peaks in those regions for ID-1144, we hypothesize that the optical cladding influences this fibre's attenuation more strongly. This could then also be an indicator for a stronger interface of core and optical cladding of ID-1144.

The presence of overtones of UV-range bands are excluded due to the usage of the 550 nm long-pass filter. Ultimately, regarding the overall polymer optical fibres' attenuation level, scattering usually dominates [36].

3.3. Laundry of the sensor

The objective of evaluating washing the sensor is to verify that the entire sensor can be reused with the embroidered polymer optical fibres embedded. This quality results in a longer life cycle and discourages continuing the currently often-followed throwaway society. It is hence very important to show that washing of the sensor is possible.

The cross-sections after washing distinctly show the continued existence core- and optical-cladding structure of the optical fibres (figure 3*c*,*d*). The statistically significant difference in diameter can be explained by the speed control of the winder, differing slightly for a full (measurement of the initial fibre characteristics) and empty (sensor production)

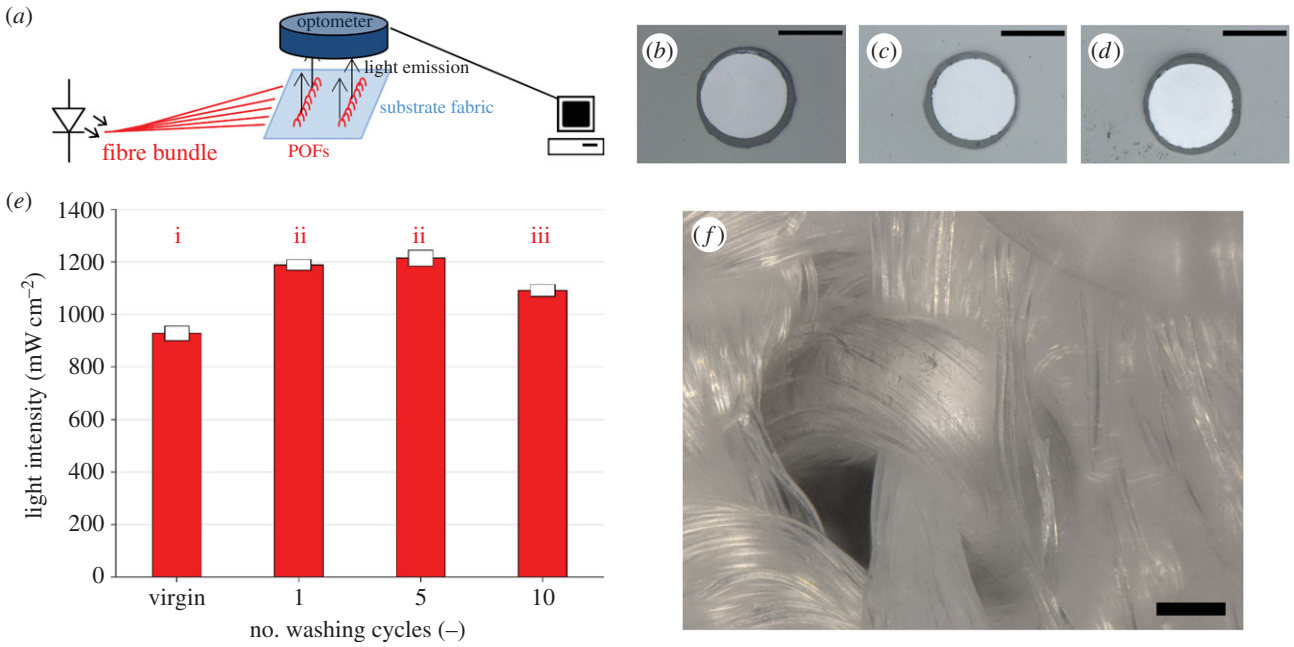

Figure 3. (*a*) Light out-coupling measurement set-up; cross-section images of the virgin fibre (*b*), a fibre washed once without detergent (*c*), and a fibre washed once with hospital-grade detergent (4 g l^{-1}) (*d*); (*e*) results for the tested fabric: The intensity is given for the untreated fabric as well as after 1, 5 and 10 washing cycles. The error bars correspond to five repeated measurements to correct for connector variation. i, ii, iii identify samples which do not show significant differences ($p < 0.05$); (*f*) three-dimensional microscope image of the embroidered polymer optical fibre within the textile. All scale bars indicate 100 µm. (Online version in colour.)

spool. The light out-coupling intensity from the textile increases after the first washing cycle (figure 3*e*). We explain this by the removal of dust which may have accumulated on the fibre during embroidery and absorbed light. Also, fluid preventing electrostatic charging at the high production speeds is washed off. The removal of droplets is also observed in microscopic images. Additionally, we observed an average of 1% shrinkage of the textile, decreasing the bending radius slightly.

The decrease for 10 washing cycles is due to the strong entangling and the subsequent disentangling of the optical fibre bundles during washing that connect to the light source and detector (figure 4*a*). However, the light intensity after 10 washing cycles still exceeds the virgin fibre set-up and shows the reusability of the system.

The low COF, which lies below that of commercial, typically used textiles in hospital applications, assures the comfort of the sensor for applications in contact with the skin. The reusability of the sensor by washing renders it a promising candidate for commercialization making the life cycle of the sensor longer.

The use of conventional textile techniques for the production of the sensor also assures its washability. As shown in figure 3*f*, the POFs are incorporated as a part of the textile patch itself. This fact is responsible for the excellent performance of the sensor even after 10 washing cycles (figure 3*e*). In comparison, other systems make use of single fibres that are prone to damage during washing cycles [5,38].

3.4. Friction analysis of the sensor

First, samples were prepared with varying covering area of POFs. Such, we verified that the introduced fibres ID-1144 act according to Amonton's second law of friction (figure 4*c*). This law states that irrespective of the embroidered area, the COF stays constant [39]. This does not hold true when strong wear plays a role in the contact situation. Hence, we can conclude that the textile sensor is not subjected to strong wear changing the real contact area from cycle to cycle. It is thus only dependent on applied load for both wet and dry conditions. Additionally, 1000 cycles allow for a judgement on the embroidering stability. A strong increase in COF would have spoken for a disassembly of the fibres from the substrate.

In comparison with different textiles conventionally used as bedsheets (cotton and cotton/polyester (50 : 50)), the POF textiles outperform both. The newly developed POF textiles can hence be used for risk patients as we can assume lower skin chafing probability. Especially in wet conditions, the water removal capability of the decubitus bedsheet in combination with fluorinated fibres shows a clear advantage [40]. Not only does the bedsheet allow for wicking, but the POFs can even enhance this effect due to their hydrophobicity [24,36,41]. When taking the increase of static COF for the bedsheet into account, the POF textile only increases by 0.023 ± 0.007 for fibre ID-1144. In comparison, the decubitus bedsheet increases on average by 0.048 ± 0.004 for the static COF. Such, the substrate contributes most to the difference in COF between wet and dry conditions. For cotton, a pilling effect can be observed, increasing the COF (figure 4*d*).

3.5. Heartbeat sensor testing

The optical fibre is bent tightly by being wound around the sewing yarn (figure 3*f*). Hence, the incorporation of the optical fibres within the textile substrate automatically ensures strong light out-coupling. The out-coupled light then passed through the tissue (schematic in figure 5*a*) and experiences scattering events and absorption by tissue and blood. When detected by the second set of optical fibres, the signal varies with each heartbeat due to the absorption of light by haemoglobin, which is stronger in larger blood volumes. This signal allows the estimation of physiological parameters such as heart rate and heart rate variabilities.

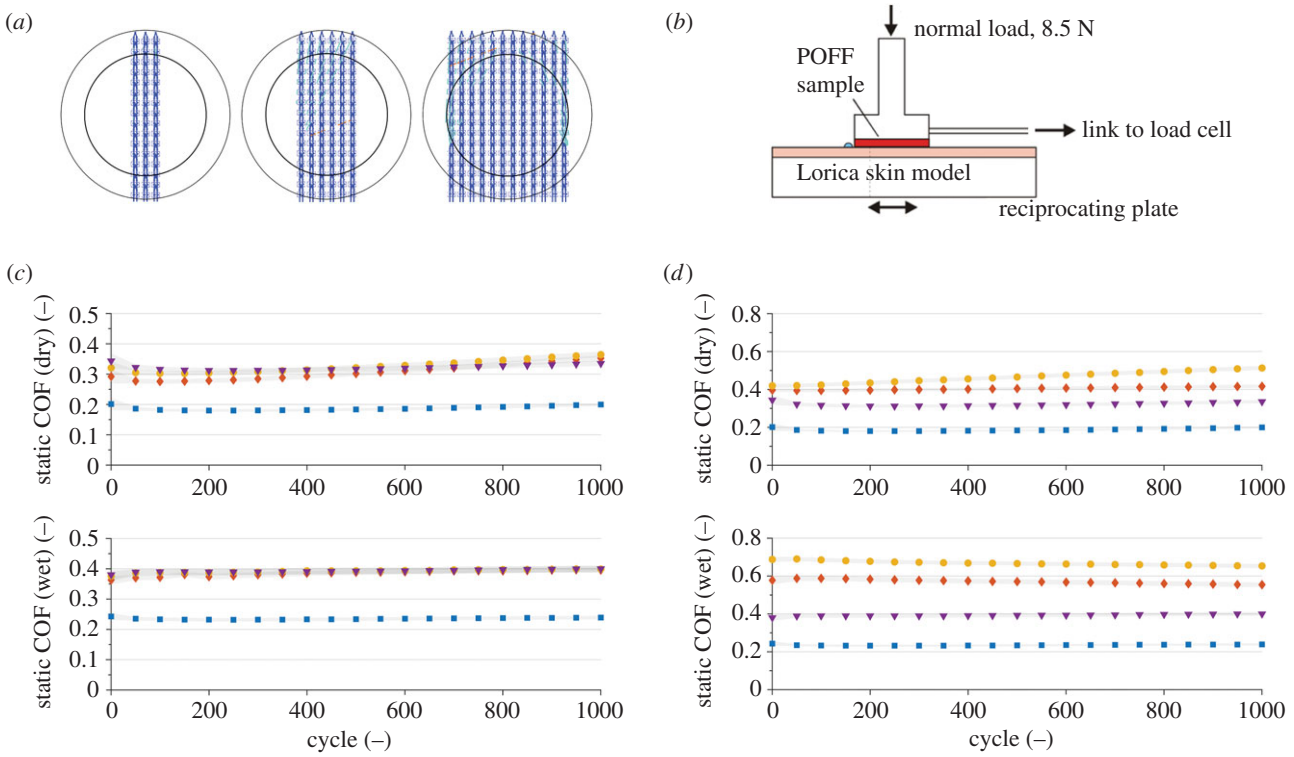

Figure 4. (*a*) Design for the friction measurements for both optical fibres ID-1144 and ID-1143. The outer circle shows the punched-out area for the friction measurements, the inner circle shows the area in contact with the skin model. (*b*) Schematic of testing set-up, the POF fabric (POFF) is tested versus a skin model at a normal load of 8.5 N. The coefficient of friction is calculated with the load cell data, adapted from [23] with permission from Elsevier. (*c*) Static coefficient of friction of fibre ID-1144 in dry (top) and wet (64 µl) (bottom) conditions with varying fibre content on the test patches. Colours/shapes correspond to the following configurations: three embroidered lines (diamonds), six embroidered lines (circles) and 12 embroidered lines (triangles) while the substrate (textile without POFs) as a reference is plotted with squares. (*d*) Static coefficient of friction of different textiles in dry (top) and wet (64 µl) (bottom) conditions. The following fabrics are compared: decubitus bedsheet (Schoeller) (blue squares), cotton/polyester (50 : 50) (diamonds), cotton (100%) (circles) and the fibre patches with fibre ID-1144 (triangles). (Online version in colour.)

Figure 5*b* shows an example of a raw PPG signal measured at the forehead with the optical fibres (reflection mode) and compared with reference measurements from fingertip PPG (transmission mode) and a raw signal plot of ECG electrodes, both measured using BIOPAC. The heart rate was calculated from the timing of the falling slopes of the PPG signals. Prior to comparison, the heart rate was further interpolated to 1 Hz and averaged over 4 s windows. Figure 5*c* shows the comparison of average heart rate when measured with the new textile-integrated optical fibre sensor and the BIOPAC PPG over the entire measurement protocol of one particular subject. The new sensor and the commercial solution were used at the same time and linked to time stamps. The highest deviations stem from motion artefacts at the end of the handgrip exercise. At these, the exhaustion of the subject is more easily transmitted to the head than the other hand (by trembling) as the second hand was placed on a table. When evaluated over the five subjects measured, the final performance shows a mean absolute error of 0.38 bpm; hence the small motion artefacts do not impede sensor performance critically. The Bland–Altman analysis shown in figure 5*d* reveals a good agreement of the fibre-based heart rate estimate when compared with the reference at the fingertip. The confidence interval suggests that the difference between the sensors is not clinically important and the sensors can hence be used interchangeably.

There have been some examples of the measurement of heartbeat by using POFs in recent years [5,8,38]. In our previous work, we successfully measured both the heartbeat as well as the oxygen saturation in the blood in reflection mode using embroidered POFs [8]. However, the system still utilized a stiff, commercial PMMA fibre for transporting light to the skin, with negative effects on the comfort of the sensor and limitations due to the inadequate mechanical properties of such fibres. Suaste-Gómez and Hernández-Rivera have also proposed a POF-based heartbeat sensor [38]. In that case, however, the sensor is used in transmission mode comparable to conventional pulse oximeters. A clip must be placed around the finger which limits the applicability of the sensor in terms of long-term monitoring. Other systems include e.g. embedded prisms for light-guiding or supplying light by silica fibres [42,43].

Our proposed system presents therefore several advantages when placed at a well-perfused area compared with the previous ones. The embroidery of soft, flexible POF on a low-friction textile guarantees comfort to the user even after long periods of use or after several friction cycles. Such a characteristic is of paramount importance to e.g. paraplegic patients, to decrease the risk of developing pressure ulcers. The set-up is also modular and allows the integration of other POF-based sensors, e.g. pressure sensors in a single textile patch, increasing the usefulness and decreasing the complexity of the system simultaneously [15].

4. Conclusion

In this paper, we demonstrated the embroidery of melt-spun polymer optical fibres into textile substrates. The bi-component, continuous melt-spinning approach for optical

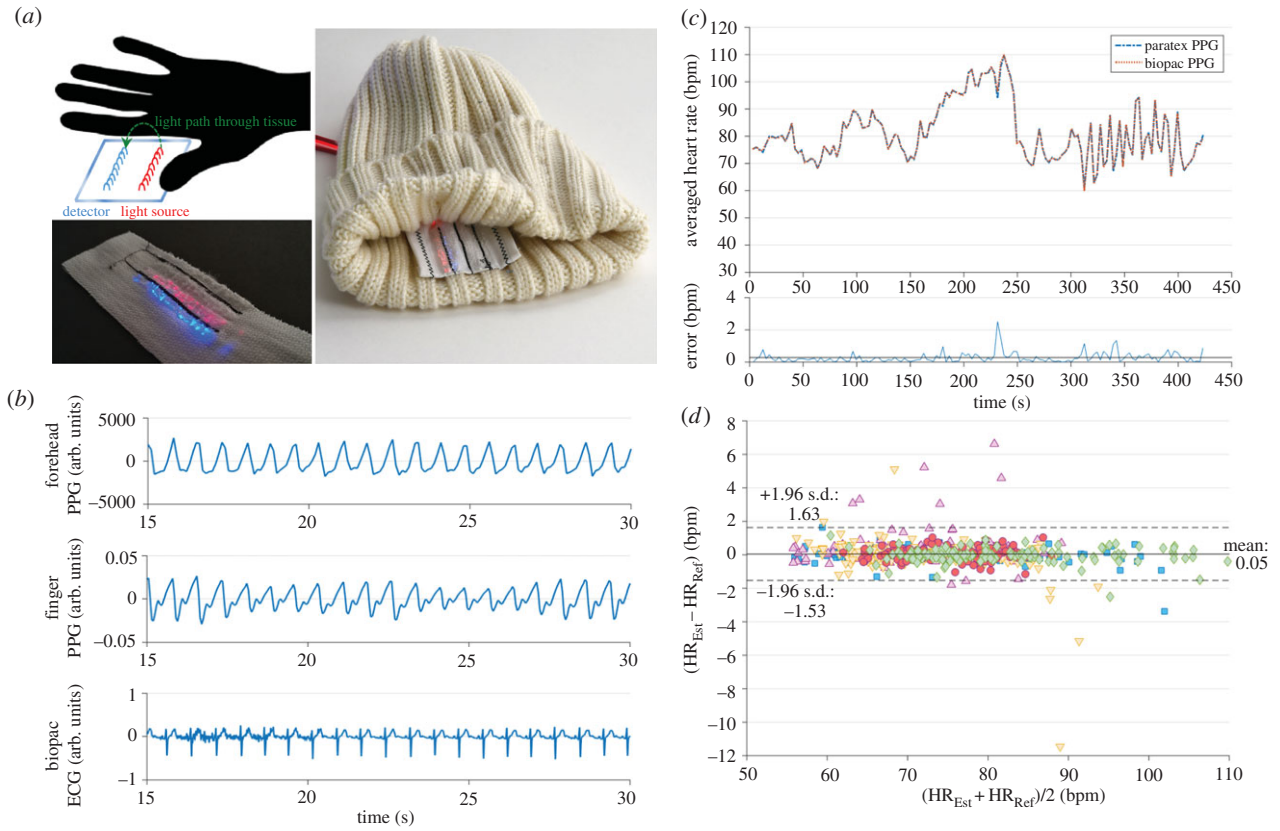

Figure 5. (*a*) Schematic of the sensing technique of the sensor in reflection mode (upper left), the sensor in close-up while illuminated (emission: red, detection: blue) (lower left), and prototype of the sensing hat (right); (*b*) raw signals measured with the polymer optical fibre sensor in reflection mode from the forehead, as well as the PPG and ECG signal from the BIOPAC sensors; (*c*) calculation of the heartrate averaged over 4 s from both, the sensor at the forehead and the BIOPAC finger clip; the average absolute error is given in the lower graph; (*d*) Bland–Altman plot showing the agreement of the fibre-based sensor (HR_{Est}) and the reference (HR_{Ref}) for five subjects (plotted with different colours and symbols).

fibres allowed producing homogeneous fibres with the most recent optimization of production parameters. A reliable core-cladding structure essential for optical fibre light transmission was achieved. We were able to also optimize the mechanical properties of our POFs. This ensured fast and reliable embroidery, decreasing the number of fibre breaks. Simultaneous embroidery of several sensors was therefore possible.

Last, we could, for the first time, present low-friction, flexible, embroidered sensors. The sensors were able to measure the heartbeat (and heart rate) in reflection at the forehead using a LED as the light source. This proof-of-principle hence demonstrates the applicability of the sensor in reflection mode at thicker body parts. In our previous work, the light source was a laser diode which introduces safety concerns when used for clinical trials in skin-contact applications [8]. An LED therefore also offers many advantages in terms of miniaturization and energy consumption, which opens the way towards a successful miniaturization and integration of such sensors into conventional textiles such as clothing or seats. Moreover, contrary to ECG electrodes, such an optical sensor does not require wetting of the skin to acquire the signal which would otherwise change dermal conditions again.

From here, we will add further wavelengths to the electronics to also record oxygen saturation in the tissue. Moreover, the set-up is modular and will also allow the incorporation of other sensing units, e.g. pressure sensors. Such textile sensors will play a fundamental role in the long-term monitoring of patients by offering a comfortable, simple and reliable way of measuring their vital signs.

Authors' contributions. B.M.Q. carried out the laboratory work and data analysis, drafted the manuscript and carried out fibre production together with R.H.; F.B. and D.F. worked on the used electronics and data acquisition; A.S.-S., G.-L.B., R.M.R., L.J.S. and M.W. designed and coordinated the study, L.F.B. carried out the statistical analysis and coordinated the study. All authors participated in the manuscript writing and gave final approval for publication.

Competing interests. We declare we have no competing interests.

Funding. This project is funded by Nano-Tera.ch (within the ParaTex and the ParaTex-Gateway project) with Swiss Confederation financing.

Acknowledgements. Gratefully acknowledged is the support of Andrés Leal (resiliency testing), Siegfried Derler and Gelu-Mariusz Rotaru (friction), Denise Mitrano (washing), and Eugen Zgraggen and Ivan Shorubalko (optical equipment). Additionally, Benno Wüst is thanked for his knowledge in fibre spinning.

References

1. Mak AFT, Zhang M, Tam EWC. 2010 Biomechanics of pressure ulcer in body tissues interacting with external forces during locomotion. In *Annual review of biomedical engineering*, vol. 12 (eds ML Yarmush, JS Duncan, ML Gray), pp. 29–53. Palo Alto, CA: Annual Reviews.

2. May JH, Bazzoli GJ, Gerland AM. 2006 Hospitals' responses to nurse staffing shortages. *Health Aff.* **25**, W316–WW23. (doi:10.1377/hlthaff.25.w316)

3. Ramella-Roman JC *et al*. 2013 Monitoring the impact of pressure on the assessment of skin perfusion and oxygenation using a novel pressure device. In *Progress in Biomedical Optics and Imaging*. Bellingham, WA: SPIE.
4. Makhsous M, Priebe M, Bankard J, Rowles D, Zeigler M, Chen D, Lin P. 2007 Measuring tissue perfusion during pressure relief maneuvers: Insights into preventing pressure ulcers. *J. Spinal Cord Med*. **30**, 497–507. (doi:10.1080/10790268.2007.11754584)
5. Quandt BM, Scherer LJ, Boesel LF, Wolf M, Bona GL, Rossi RM. 2015 Body-monitoring and health supervision by means of optical fiber-based sensing systems in medical textiles. *Adv. Healthcare Mater*. **4**, 330–355. (doi:10.1002/adhm.201400463)
6. Ziemann O, Krauser J, Zamzow PE, Daum W. 2003 *POF-polymer optical fibers for data communication*. Berlin, Germany: Springer Science & Business Media.
7. Tanio N, Koike Y. 2000 What is the most transparent polymer? *Polym. J*. **32**, 43–50. (doi:10.1295/polymj.32.43)
8. Krehel M, Wolf M, Boesel LF, Rossi RM, Bona G-L, Scherer LJ. 2014 Development of a luminous textile for reflective pulse oximetry measurements. *Biomed. Optics Express* **5**, 2537–2547. (doi:10.1364/BOE.5.002537)
9. Quandt BM, Hufenus R, Weisse B, Braun F, Wolf M, Scheel-Sailer A, Bona G-L, Rossi RM, Boesel LF. 2017 Optimization of novel melt-extruded polymer optical fibers designed for pressure sensor applications. *Eur. Polym. J*. **88**, 44–55. (doi:10.1016/j.eurpolymj.2016.12.032)
10. Ramalho A, Szekeres P, Fernandes E. 2013 Friction and tactile perception of textile fabrics. *Tribol. Int*. **63**, 29–33. (doi:10.1016/j.triboint.2012.08.018)
11. Bertaux E, Derler S, Rossi RM, Zeng X, Koehl L, Ventenat V. 2010 Textile, physiological, and sensorial parameters in sock comfort. *Textile Res. J*. **80**, 1803–1810. (doi:10.1177/0040517510369409)
12. Powers JG, Higham C, Broussard K, Phillips TJ. 2016 Wound healing and treating wounds chronic wound care and management. *J. Am. Acad. Dermatol*. **74**, 607–625. (doi:10.1016/j.jaad.2015.08.070)
13. Reducing cost and improving the quality of health care. 2013. Washington, DC: The White House. See https://www.whitehouse.gov/sites/default/files/docs/erp2013/ERP2013_Chapter_5.pdf.
14. Soukup R, Hamacek A, Mracek L, Reboun J (eds). 2014 Textile based temperature and humidity sensor elements for healthcare applications. In *Proc. of the 2014 37th International Spring Seminar on Electronics Technology, ISSE 2014*. Piscataway, NJ: IEEE.
15. Krehel M, Rossi RM, Bona G-L, Scherer LJ. 2013 Characterization of flexible copolymer optical fibers for force sensing applications. *Sensors* **13**, 11 956–11 968. (doi:10.3390/s130911956)
16. Krehel M, Schmid M, Rossi R, Boesel L, Bona G-L, Scherer L. 2014 An optical fibre-based sensor for respiratory monitoring. *Sensors* **14**, 13 088–130 101. (doi:10.3390/s140713088)
17. Reifler FA, Hufenus R, Krehel M, Zgraggen E, Rossi RM, Scherer LJ. 2014 Polymer optical fibers for textile applications—bicomponent melt spinning from cyclic olefin polymer and structural characteristics revealed by wide angle X-ray diffraction. *Polymer* (*UK*) **55**, 5695–5707.
18. White WR, Blyler Jr LL, Ratnagiri R, Park M (eds). 2004 Manufacture of perfluorinated plastic optical fibers. In *Optical Fiber Communication Conference, OFC 2004*. Los Angeles, CA: OFC.
19. Hufenus R, Reifler FA, Maniura-Weber K, Spierings A, Zinn M. 2012 Biodegradable bicomponent fibers from renewable sources: melt-spinning of poly(lactic acid) and poly[(3-hydroxybutyrate)-co-(3-hydroxyvalerate)]. *Macromol. Mater. Eng*. **297**, 75–84. (doi:10.1002/mame.201100063)
20. Leal AA, Mohanty G, Reifler FA, Michler J, Hufenus R. 2014 Mechanical response of melt-spun amorphous filaments. *Sci. Technol. Adv. Mater*. **15**, 035016. (doi:10.1088/1468-6996/15/3/035016)
21. Thorlabs. 2016 Unmounted Longpass Colored Glass Filters: Thorlabs. See http://www.thorlabs.de/newgrouppage9.cfm?objectgroup_id=999&pn=FGL550#3709.
22. Zgraggen E. 2012 *Fabrication and system integration of single-mode polymer optical waveguides*. Zurich, Switzerland: ETH Zurich.
23. Derler S, Rao A, Ballistreri P, Huber R, Scheel-Sailer A, Rossi RM. 2012 Medical textiles with low friction for decubitus prevention. *Tribol. Int*. **46**, 208–214. (doi:10.1016/j.triboint.2011.03.011)
24. Derler S, Schrade U, Gerhardt LC. 2007 Tribology of human skin and mechanical skin equivalents in contact with textiles. *Wear* **263**, 1112–1116. (doi:10.1016/j.wear.2006.11.031)
25. Gerhardt LC, Schiller A, Müller B, Spencer ND, Derler S. 2009 Fabrication, characterisation and tribological investigation of artificial skin surface lipid films. *Tribol. Lett*. **34**, 81–93. (doi:10.1007/s11249-009-9411-0)
26. Gerhardt L-C, Strässle V, Lenz A, Spencer ND, Derler S. 2008 Influence of epidermal hydration on the friction of human skin against textiles. *J. R. Soc. Interface* **5**, 1317–1328. (doi:10.1098/rsif.2008.0034)
27. Mitrano DM, Arroyo Rojas Dasilva Y, Nowack B. 2015 Effect of variations of washing solution chemistry on nanomaterial physicochemical changes in the laundry cycle. *Environ. Sci. Technol*. **49**, 9665–9673. (doi:10.1021/acs.est.5b02262)
28. Allen J. 2007 Photoplethysmography and its application in clinical physiological measurement. *Physiol. Meas*. **28**, R1–R39. (doi:10.1088/0967-3334/28/3/R01)
29. Meredith DJ, Clifton D, Charlton P, Brooks J, Pugh CW, Tarassenko L. 2012 Photoplethysmographic derivation of respiratory rate: a review of relevant physiology. *J. Med. Eng. Technol*. **36**, 1–7. (doi:10.3109/03091902.2011.638965)
30. R: A Language and Environment for Statistical Computing. 2012. http://www.R-project.org.
31. Fox J. 2005 The R Commander: a basic statistics graphical user interface to R. *J. Stat. Softw*. **14**, 1–42.
32. ZeonCorporation. Datasheet Zeonor 1020R. 2016 See http://www.zeon.co.jp/content/200181692.pdfaccessed 9 March, 2016.
33. Dyneon LLC. 2016 Datasheet THVP 2030GX. http://multimedia.3m.com/mws/media/6232960/thvp-2030g-x.pdf, accessed 9 March 2016.
34. Nadella HP, Spruiell JE, White JL. 1978 Drawing and annealing of polypropylene fibers: structural changes and mechanical properties. *J. Appl. Polym. Sci*. **22**, 3121–3133. (doi:10.1002/app.1978.070221108)
35. Khanarian G, Celanese H. 2001 Optical properties of cyclic olefin copolymers. *Optice* **40**, 1024–1029. (doi:10.1117/1.1369411)
36. Groh W. 1988 Overtone absorption in macromolecules for polymer optical fibers. *Die Makromolekulare Chemie* **189**, 2861–2874. (doi:10.1002/macp.1988.021891213)
37. Zhou M. 2002 Low-loss polymeric materials for passive waveguide components in fiber optical telecommunication. *Optice* **41**, 1631–1643. (doi:10.1117/1.1481895)
38. Suaste-Gómez E, Hernández-Rivera D, Sánchez-Sánchez A, Villarreal-Calva E. 2014 Electrically insulated sensing of respiratory rate and heartbeat using optical fibers. *Sensors* **14**, 21523. (doi:10.3390/s141121523)
39. Cheong WCD, Yong AM. 2013 Probing the complexities of friction in submicron contacts between two pristine surfaces. In *Nano-tribology and materials in MEMS* (eds KS Sinha, N Satyanarayana, CS Lim), pp. 199–213. Heidelberg, Germany: Springer.
40. Derler S, Rotaru GM, Ke W, Issawi-Frischknecht LE, Kellenberger P, Scheel-Sailer A, Rossi FM. 2014 Microscopic contact area and friction between medical textiles and skin. *J. Mech. Behav. Biomed. Mater*. **38**, 114–125. (doi:10.1016/j.jmbbm.2014.06.014)
41. Rotaru GM, Pille D, Lehmeier FK, Stämpfli R, Scheel-Sailer A, Rossi RM, Derler S. 2013 Friction between human skin and medical textiles for decubitus prevention. *Tribol. Int*. **65**, 91–96. (doi:10.1016/j.triboint.2013.02.005)
42. Witt J *et al*. 2013 Personal protective equipment with integrated POF sensors2013; Krakow.
43. Rothmaier M, Selm B, Spichtig S, Haensse D, Wolf M. 2008 Photonic textiles for pulse oximetry. *Opt Exp*. **16**, 12 973–12 986. (doi:10.1364/OE.16.012973)